

# Wafer-Scale and Wrinkle-Free Epitaxial Growth of Single-Orientated Multilayer Hexagonal Boron Nitride on Sapphire

A-Rang Jang,<sup>†,‡,§</sup> Seokmo Hong,<sup>†</sup> Chohee Hyun,<sup>‡</sup> Seong In Yoon,<sup>‡</sup> Gwangwoo Kim,<sup>‡</sup> Hu Young Jeong,<sup>†</sup> Tae Joo Shin,<sup>†</sup> Sung O. Park,<sup>†</sup> Kester Wong,<sup>†</sup> Sang Kyu Kwak,<sup>†,¶</sup> Noejung Park,<sup>†,¶</sup> Kwangnam Yu,<sup>○</sup> Eunjin Choi,<sup>○</sup> Artem Mishchenko,<sup>◆</sup> Freddie Withers,<sup>◆</sup> Kostya S. Novoselov,<sup>◆</sup> Hyunseob Lim,<sup>\*,†,§,||</sup> and Hyeon Suk Shin<sup>\*,†,‡,§,||</sup>

<sup>†</sup>Department of Chemistry, <sup>‡</sup>Department of Energy Engineering, <sup>§</sup>Low Dimensional Carbon Materials, <sup>¶</sup>UNIST Central Research Facilities (UCRF), <sup>||</sup>Department of Physics, and <sup>○</sup>School of Energy and Chemical Engineering, Ulsan National Institute of Science and Technology (UNIST), UNIST-gil 50, Ulsan 44919, Republic of Korea

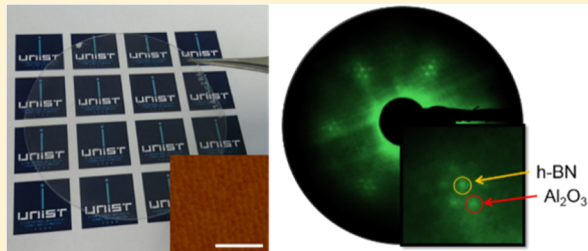
<sup>◆</sup>Center for Multidimensional Carbon Materials, Institute of Basic Science (IBS), Ulsan 44919, Republic of Korea

<sup>○</sup>Department of Physics, University of Seoul, Seoul 02504, Republic of Korea

<sup>◆</sup>School of Physics and Astronomy, University of Manchester, Manchester M13 9PL, United Kingdom

## Supporting Information

**ABSTRACT:** Large-scale growth of high-quality hexagonal boron nitride has been a challenge in two-dimensional-material-based electronics. Herein, we present wafer-scale and wrinkle-free epitaxial growth of multilayer hexagonal boron nitride on a sapphire substrate by using high-temperature and low-pressure chemical vapor deposition. Microscopic and spectroscopic investigations and theoretical calculations reveal that synthesized hexagonal boron nitride has a single rotational orientation with AA' stacking order. A facile method for transferring hexagonal boron nitride onto other target substrates was developed, which provides the opportunity for using hexagonal boron nitride as a substrate in practical electronic circuits. A graphene field effect transistor fabricated on our hexagonal boron nitride sheets shows clear quantum oscillation and highly improved carrier mobility because the ultraflatness of the hexagonal boron nitride surface can reduce the substrate-induced degradation of the carrier mobility of two-dimensional materials.



**KEYWORDS:** Hexagonal boron nitride, chemical vapor deposition, ammonia borane, sapphire substrate

Two-dimensional (2D) atomic crystals have recently received considerable attention as building blocks for postsilicon integrated electronic circuits. Owing to their electronic properties, graphene, and transition metal dichalcogenides (TMDs) have been widely investigated for use as electrodes or semiconducting channels.<sup>1–7</sup> Hexagonal boron nitride (h-BN), a 2D insulator with a wide band gap (5–6 eV), has been regarded as a good candidate for dielectric layer or insulating barrier, because of its atomically flat surface and the lack of dangling bonds and charge impurities at the surface.<sup>8–10</sup> Ultrahigh mobility of graphene was demonstrated in graphene transistors using h-BN as a dielectric,<sup>11–16</sup> and a field effect tunneling transistor (FETT) of vertical architecture was also recently developed using h-BN as a tunneling barrier.<sup>17,18</sup> Although bulk h-BN crystals for mechanical exfoliation have been synthesized by a metal-BN solvent-assisted method under high temperature (1500–1750 °C) and high pressure (4.0–5.5 GPa),<sup>19</sup> their size and three-dimensional morphology limits their application in practical 2D-electronic devices. Thus, the growth of 2D h-BN in a large area is strongly required. A number of methods based on chemical vapor deposition

(CVD) were reported using various substrates, such as Cu,<sup>20–24</sup> Ni,<sup>25,26</sup> Pt,<sup>27–29</sup> Fe,<sup>30,31</sup> and SiO<sub>2</sub>.<sup>32</sup> Especially, multilayer h-BN growth with uniform thickness is also one of the important requirements in 2D h-BN, because monolayer h-BN is not thick enough to inhibit the electron transport through the h-BN layer in the surface normal direction and any influence of substrate morphology or roughness underneath the h-BN. Recently, Kim et al. reported the highly improved carrier mobility in 2D materials transferred on CVD-grown multilayer h-BN.<sup>30</sup> However, h-BN sheets grown by these methods consist of randomly oriented multi-h-BN grains, and grain boundaries between domains and wrinkle formation are generally observed. These degrade the quality of h-BN and result in a larger surface roughness compared to mechanically exfoliated h-BN. Therefore, wrinkle-free and single crystalline multilayer h-BN in large

**Received:** March 10, 2016

**Revised:** April 22, 2016

**Published:** April 27, 2016



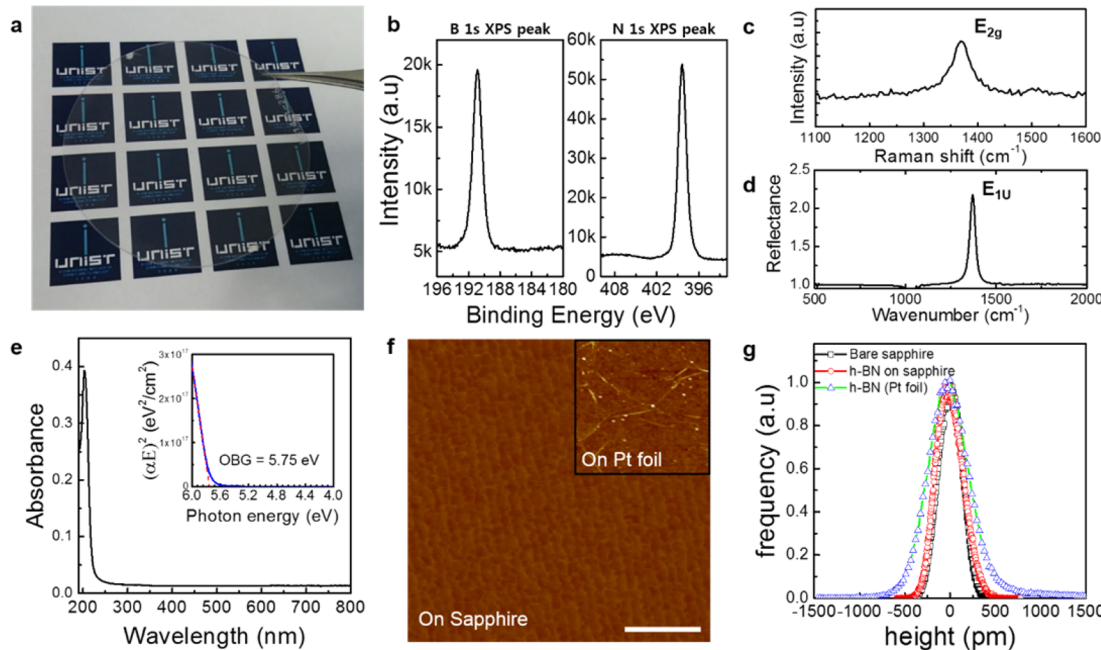


**Figure 1.** Microscopic and spectroscopic characterizations of EM-h-BN. (a) A photograph of wafer-scale EM-h-BN on sapphire substrate. (b) XPS spectrum of EM-h-BN on sapphire substrate. (c) Raman spectrum and (d) FTIR of EM-h-BN. (e) UV-visible absorption spectra and (inset) optical band gap analysis. (f) AFM image of EM-h-BN on sapphire substrate, and (inset) monolayer h-BN grown on Pt foil. Scale bar is 500 nm. (g) Histogram of the height distribution (surface roughness) of EM-h-BN and h-BN sheet grown on Pt foil measured by AFM.

area growth has been a challenge, as is the case with graphene growth.

The wafer-scale growth of single-crystalline graphene<sup>33</sup> and polycrystalline WS<sub>2</sub><sup>34</sup> has been achieved recently. However, to the best of our knowledge the wafer-scale growth of h-BN has not yet been demonstrated. Herein, we demonstrate the epitaxial growth of multilayer h-BN on a 2-in. sapphire wafer by low-pressure CVD method. The grown single-oriented multilayer h-BN does not exhibit any wrinkle structure. Well-defined arrangement of h-BN on c-plane sapphire enables the single orientation of h-BN, and partially charged B and N atoms result in AA' stacking order rather than the randomly stacking order (turbostratic stacked), which is normally observed in multilayer graphene during CVD growth with neutrally charged C atoms. The small difference in the thermal expansion coefficients between h-BN and sapphire suppresses the wrinkle structure on the surface.<sup>35,36</sup> Furthermore, a facile method for transfer of h-BN onto other substrates developed in this work enables reusability of the sapphire substrate.

The (i) wafer-scale, (ii) wrinkle-free, (iii) and AA' stacking multilayer h-BN with (iv) single orientation was (v) epitaxially grown on a sapphire substrate by high-temperature and low-pressure CVD (HT/LP CVD). Ammonia borane (NH<sub>3</sub>BH<sub>3</sub>) used as a precursor was heated at 130 °C, and then borazine gas decomposed from NH<sub>3</sub>BH<sub>3</sub> can be introduced into the alumina tube by the carrier gases (10 sccm for Ar and 10 sccm for H<sub>2</sub>) (Figure S1).<sup>37</sup> The sapphire substrate was placed at the center of the alumina tube, which was heated up to 1400 °C. Figure 1a shows the highly transparent multilayer h-BN sheets grown on a 2-in. sapphire wafer (EM-h-BN: epitaxially grown multilayer h-BN on sapphire). To characterize EM-h-BN, various spectroscopic methods were first carried out. X-ray photoemission spectroscopy (XPS) reveals that the B/N atomic ratio in the sample is 1:0.96 (Figure 1b and Figure S2), and the highly symmetric peaks of B 1s and N 1s photoelectrons at

190.9 and 398.5 eV indicate that the sample was composed only of sp<sup>2</sup>-hybridized B and N atoms.<sup>26,38</sup> The sharp E<sub>2g</sub> phonon mode (in-plane) at 1372 cm<sup>-1</sup> in the Raman spectrum (Figure 1c) and the E<sub>1u</sub> B–N stretching mode (in-plane) at 1370.8 cm<sup>-1</sup> in the Fourier transform infrared (FT-IR) spectrum (Figure 1d) indicate the high crystallinity of the EM-h-BN sheets, and the absence of the out-of-plane mode near 760 cm<sup>-1</sup> (A<sub>2u</sub> mode) in the FT-IR spectrum confirms that the as-grown EM-h-BN is parallel to the sapphire substrate. The FTIR spectra of the EM-h-BN grown by CVD and of the transferred EM-h-BN are the same as those for the mechanically exfoliated h-BN (Figure S3). (The transfer of EM-h-BN will be discussed later on). The UV-visible absorption spectrum reveals an optical band gap of 5.75 eV, which is calculated using Tauc's eq (Figure 1e). This value is a slightly lower than the theoretically expected value for single layer h-BN (6.0 eV), because the interlayer interaction in EM-h-BN results in a more dispersed electronic structure, which reduces its band gap. The surface morphology of EM-h-BN was confirmed by atomic force microscopy (AFM), as shown in Figure 1f. A highly smooth surface without any wrinkle structures is observed, and the surface morphology with atomic steps is considered to be a reflection of the underlying sapphire surface that the EM-h-BN was projected onto (see Figure 1f and compare it with the AFM image of bare sapphire in Figure S4a). The wrinkle-free surface of EM-h-BN is anomalous compared to that of h-BN sheets grown on metal substrates, where wrinkle formation is generally observed owing to the difference in thermal expansion coefficient between h-BN and the metal substrate. In fact, numerous wrinkles are observed in the AFM image of monolayer h-BN grown on Pt foil at 1100 °C (inset of Figure 1f). Histograms of the height distribution measured by AFM also reveal that EM-h-BN has a highly smooth surface (root-mean-square roughness ( $R_z$ ) = 0.169 nm) similar to that of bare sapphire substrate ( $R_z$  = 0.128 nm, Figure

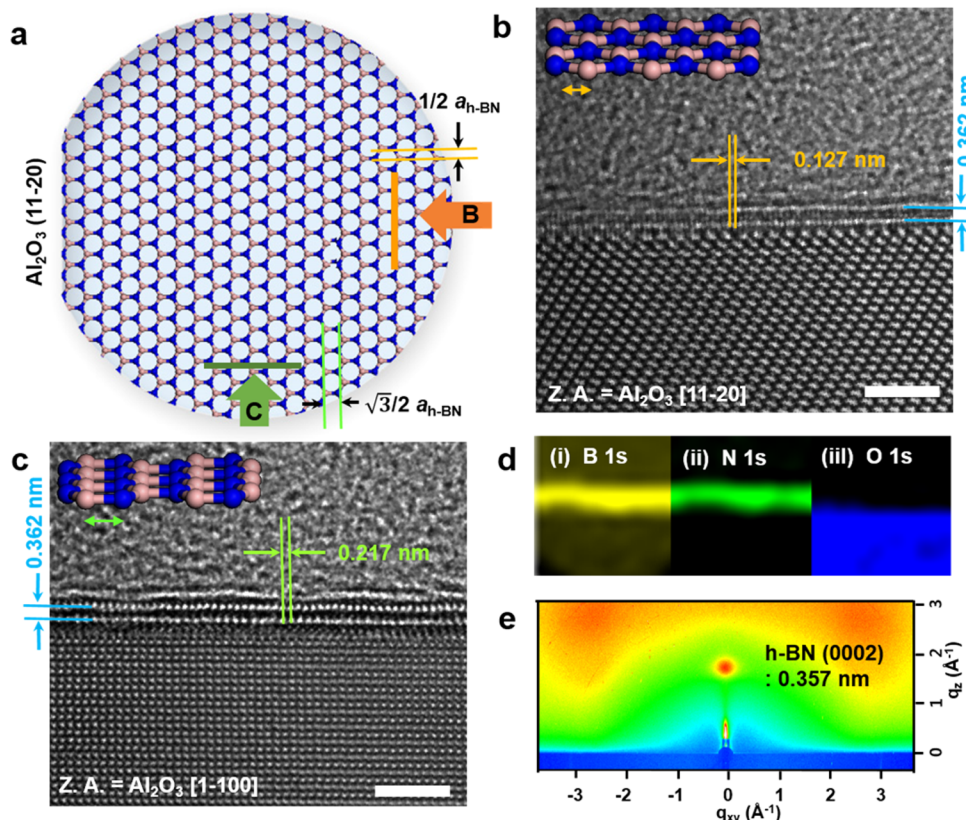


**Figure 2.** TEM and GI-WAXD analysis of EM-h-BN. (a) Schematic illustration of epitaxial grown h-BN on sapphire substrate. An HR-TEM image of multilayer h-BN grown (b) perpendicular to  $\text{Al}_2\text{O}_3$  (11̄20) and (c) parallel to  $\text{Al}_2\text{O}_3$  (11̄20). The scale bars are 2 nm. (d) EF-TEM images for B, N, and O 1s. (e) GI-WAXD result of h-BN on sapphire substrate.

S4a), while h-BN grown on Pt foil exhibits larger surface roughness ( $R_z = 1.09$  nm) (Figure 1g). We also attempted to grow h-BN on SiO<sub>2</sub>/Si but this was done at a lower temperature (1100 °C) owing to the low melting point of Si. Note that the SiO<sub>2</sub>/Si substrate cannot withstand high temperatures of up to 1400 °C. In this control experiment, h-BN particles were only grown on SiO<sub>2</sub>/Si (Figure S4c), and their randomly oriented polycrystalline structure was confirmed by HR-TEM (Figure S5). To investigate the effects of growth temperature, EM-h-BN was also grown from 1100 to 1300 °C. At 1100, 1200, and 1300 °C, h-BN particles were only grown on a sapphire substrate without any sheet structures (Figure S4d–f), and their Raman spectra indicate low crystallinity (Figure S4j–l). These results indicate that a higher growth temperature is necessary for high crystalline EM-h-BN growth on sapphire, because sapphire has a negligible catalytic effect compared to metal substrates. We believe that this catalyst-free process facilitates the growth of additional growth of upper h-BN layers at high temperature, even on the pregrown h-BN surface. However, h-BN growth is limited to a monolayer in the case of a catalyst (metal)-assisted process because further growth cannot occur on top of the h-BN surface in the absence of a catalyst effect.<sup>39,40</sup>

Cross-sectional high-resolution transmission electron microscopy (HR-TEM) was performed in order to confirm the number of layers in EM-h-BN over a large area (Figure S6a). The number of layers was confirmed to be 2–6. Even though the number of layers was not controlled, it was almost uniform over the entire surface of one sample. As shown in Figure 2a, two types of samples were prepared in different directions by

the focused ion beam (FIB) technique. One (Figure 2b) is perpendicular to  $\text{Al}_2\text{O}_3$  (11̄20) (orange, noted “B” in Figure 2a), and the other (Figure 2c) is parallel to  $\text{Al}_2\text{O}_3$  (11̄20) (green, noted “C” in Figure 2a), thus indicating different zone axes of  $\text{Al}_2\text{O}_3$  as (11̄20) and (11̄00), respectively. Interestingly, Figure 2b,c shows different lattice spacing values of h-BN in the lateral direction, 0.127 nm in Figure 2b and 0.217 nm in Figure 2c. The values are well matched with  $1/2 a_{\text{h-BN}}$  ( $1/2 \times 0.252$  nm = 0.126 nm) and  $\sqrt{3}/2 a_{\text{h-BN}}$  ( $\sqrt{3}/2 \times 0.252$  nm = 0.218 nm), corresponding to lattice spacing in zigzag and armchair directions of h-BN, respectively, as shown in Figure 2a. These results suggest that h-BN has a single-orientation of R30° and the direction of  $\text{Al}_2\text{O}_3$  unit vector ( $\text{Al}_2\text{O}_3$  ⟨11̄20⟩) is perpendicular to the direction of the h-BN unit vector (zigzag direction). If the h-BN sample consists of multioriented grains, various lattice spacing values, including  $1/2 a_{\text{h-BN}}$  (zigzag) and  $\sqrt{3}/2 a_{\text{h-BN}}$  (armchair), should be simultaneously observed regardless of the zone axis of the  $\text{Al}_2\text{O}_3$  substrate. In the HR-TEM image of a thicker EM-h-BN sample, 2D fast Fourier transform (2D-FFT) patterns were obtained from the EM-h-BN region and  $\text{Al}_2\text{O}_3$ . The zone axes in the EM-h-BN (11̄00) and  $\text{Al}_2\text{O}_3$  regions (11̄20) of the patterns were different, thus revealing that EM-h-BN is rotated by 30° with respect to the sapphire substrate (Figure S6b). Energy-filtered TEM (EF-TEM) images (Figure 2d) for B, N, and O 1s confirm that the h-BN layers are grown on the sapphire substrate. In both HR-TEM images (Figure 2b,c), the atomic positions in each layer are almost identical, and this reveals the AA or AA' stacking order in EM-h-BN. It is noted that AA' is the most appropriate for our sample, considering the layer–layer interaction in h-BN

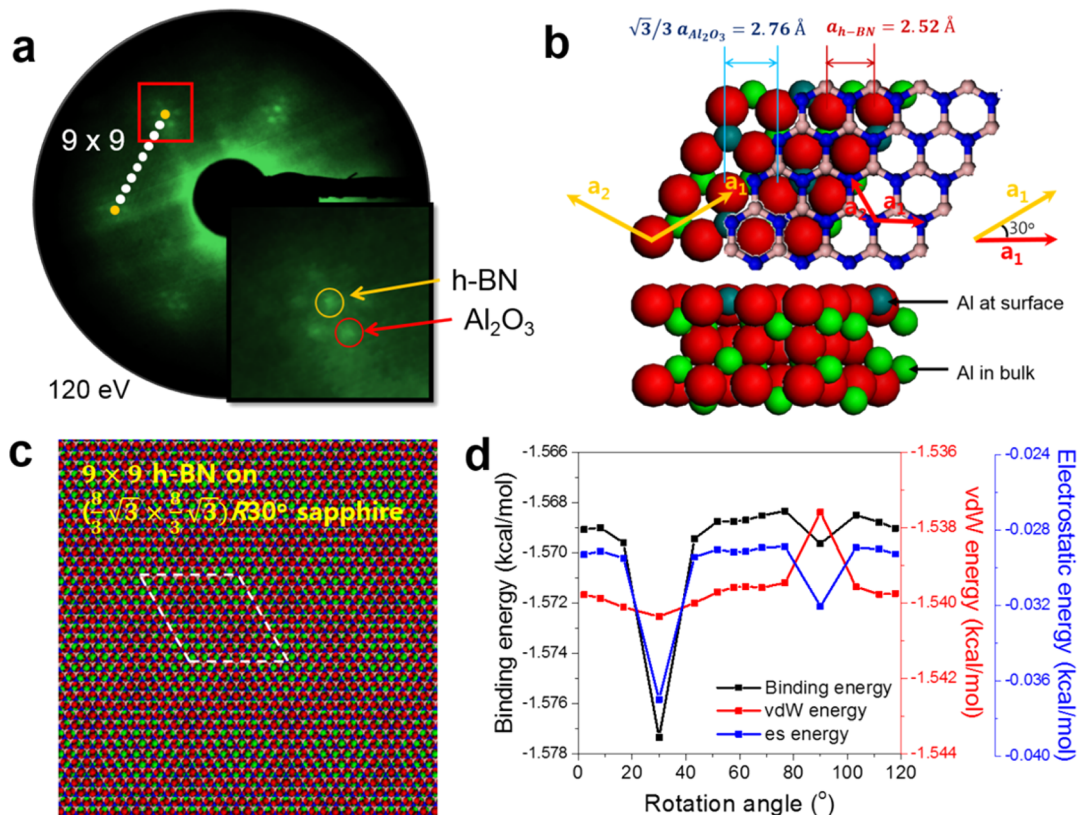


**Figure 3.** Estimation of rotational orientation on EM-h-BN. (a) LEED pattern of single-oriented h-BN grown on sapphire substrate at 120 eV. The spots marked with yellow and red circles in zoomed-in LEED pattern (inset) correspond  $a_{h-BN} = 2.52 \text{ \AA}$  (unit vector) and  $\sqrt{3}/3 a_{Al_2O_3} = 2.76 \text{ \AA}$  (O–O distance), respectively, which are displayed in panel b. (b) Atomic resolution scheme for R30° orientation. Red, green, salmon-color, and blue spheres stand for oxygen, aluminum, boron, and nitrogen elements. (c) Simulated Moiré superstructure of the h-BN on half Al-terminated Al<sub>2</sub>O<sub>3</sub> surface. (d) Binding energy, van der Waals energy, and electrostatic energy between h-BN and oxygen-terminated Al<sub>2</sub>O<sub>3</sub> surface by MD simulation according to rotational angle.

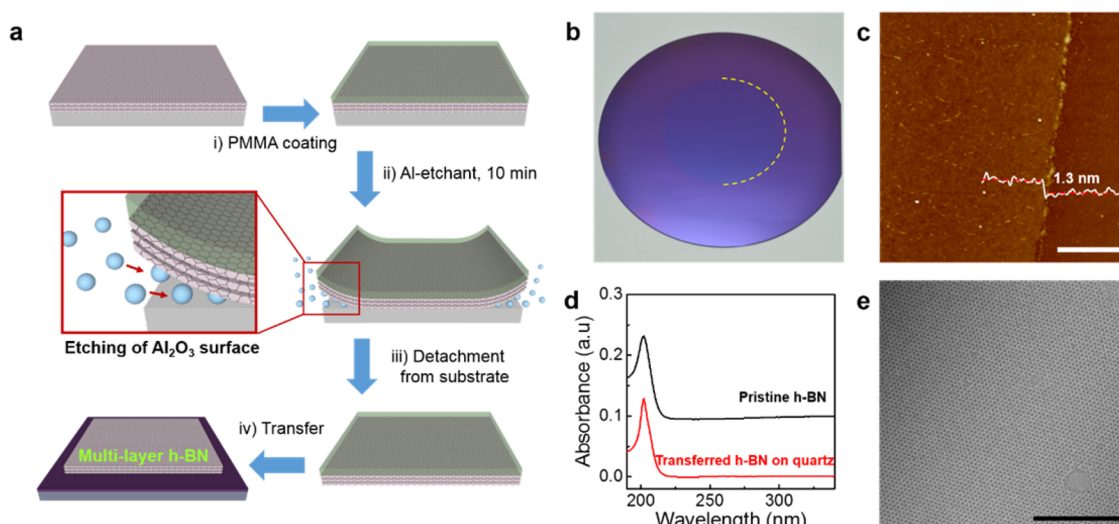


**Figure 4.** Transfer process of EM-h-BN onto other substrate. (a) Schematic illustration of EM-h-BN transfer process. (b) Photograph of the 2-in. EM-h-BN sheet transferred onto a 4-in. SiO<sub>2</sub>/Si wafer. (c) AFM image of transferred EM-h-BN. Scale bar is 500 nm. (d) UV-visible spectra of pristine EM-h-BN on sapphire and transferred EM-h-BN on quartz substrate. (e) HR-TEM image of AA' stacked EM-h-BN. Scale bar is 5 nm.

with respect to stacking types.<sup>41,42</sup> Figure 2e shows the grazing-incidence wide-angle X-ray diffraction (GI-WAXD) pattern, which provides information on the surface-sensitive crystal information on EM-h-BN. The interlayer distance measured by GI-WAXD is 0.357 nm, which is slightly larger than that of bulk

h-BN (0.330 nm) possibly due to the corrugation originated by the interaction with the sapphire substrates.

To clarify the preferred single-orientation of EM-h-BN, the low-energy electron diffraction (LEED) pattern was obtained on the whole area of the sample (Figure 3a). The LEED pattern

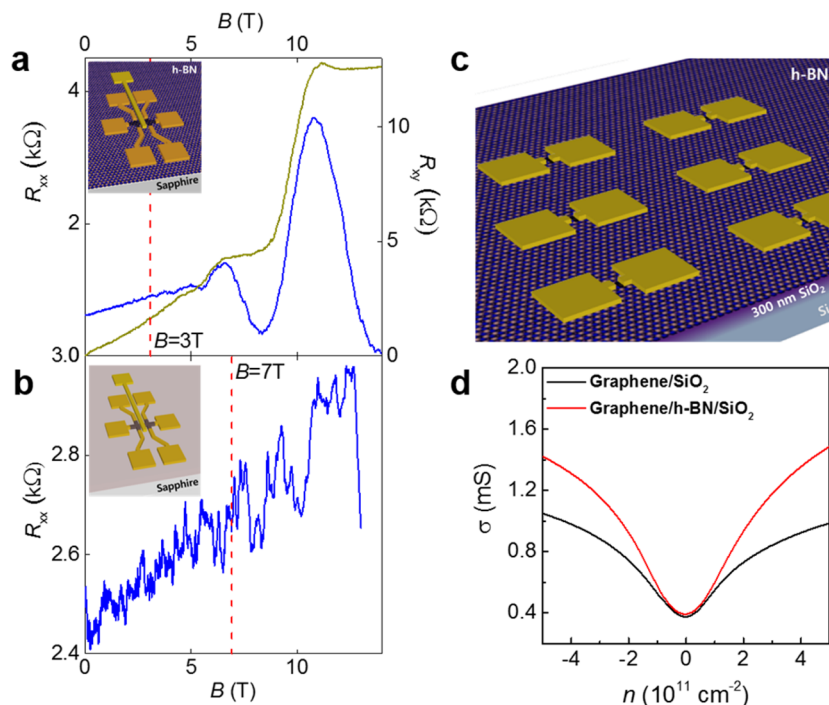


**Figure 5.** Quantum oscillations and electric field effect in graphene on EM-h-BN/sapphire substrate. SdH oscillation of graphene on as-grown EM-h-BN/sapphire (a) and bare sapphire (b) substrates. The data are taken at zero gate voltage at the residual constant carrier concentration  $n = -3.9 \times 10^{12} \text{ cm}^{-2}$  (a) and  $-1.2 \times 10^{12} \text{ cm}^{-2}$  (b).  $T = 1.5\text{K}$ , the negative sign of the carrier concentration indicates the hole doping. Noise on (b) is reproducible and is most probably the universal conductance fluctuations. (c) A schematic diagram of graphene FETs on transferred EM-h-BN/ $300 \text{ nm SiO}_2$ /Si substrate. (d) Conductance of graphene FETs on bare  $\text{SiO}_2$ /Si and transferred EM-h-BN/ $\text{SiO}_2$ /Si as a function of carrier density,  $n$ .

shows hexagonally arranged spots, rather than ring-shaped patterns, all over the sample, which reveals the single-orientation of h-BN layers over the entire sample. In addition, hexagonal satellite spots (Moiré spots), whose  $k$  vector is one-ninth that of the h-BN  $k$  vector, indicates the  $(9 \times 9)$  h-BN superstructure. Taker's Rule has predicted that the most stable  $\text{Al}_2\text{O}_3$  surface is terminated by half an Al layer, which can be used for understanding the exact orientation of EM-h-BN on sapphire substrate (Figure 3b).<sup>43,44</sup> Considering  $a_{\text{h-BN}} = 2.52 \text{ \AA}$  and  $\sqrt{3}/3a_{\text{Al}_2\text{O}_3} = 2.76 \text{ \AA}$ , the orientation of the epitaxial h-BN sheet was revealed to be  $9 \times 9$  h-BN ( $9 \times 2.52 \text{ \AA} = 22.68 \text{ \AA}$ ) unit cells on  $((\frac{8}{3}\sqrt{3} \times \frac{8}{3}\sqrt{3})R30^\circ$  sapphire supercell ( $8 \times 2.76 \text{ \AA} = 22.08 \text{ \AA}$ ), and this indicates that EM-h-BN was contracted by 2.6% ( $22.68 \text{ \AA}$  (h-BN)  $\times 97.3\% = 22.08 \text{ \AA}$  ( $\text{Al}_2\text{O}_3$ )) in the lateral direction. However, the actual strain in EM-h-BN might be smaller than 2.6%, because the corrugation of h-BN sheet can mitigate the strain. Periodic density functional theory (DFT) calculation and molecular dynamics (MD) simulation were performed in order to unveil the origin of the preferred rotational angle. The partial charges at each element were first calculated based on DFT calculations with the experimentally estimated superstructure, i.e.,  $(9 \times 9)$  h-BN on  $(\frac{8}{3}\sqrt{3} \times \frac{8}{3}\sqrt{3})R30^\circ$  sapphire (Figure 3c). Then, the binding energy between the h-BN layer and the half Al-terminated  $\text{Al}_2\text{O}_3$  surface was calculated by MD simulation with respect to the rotational angle ( $R\theta$ ) (Table S1) and the calculated values are plotted in Figure 3d. The calculation results (black) demonstrate that the  $R30^\circ$  is the most stable orientation, which is consistent with experimental observations. In particular, the contributions of van der Waals (vdW) energy (red) and electrostatic (ES) energy (blue) to the total binding energy are

plotted in Figure 3d. Even though the total binding energy is predominantly influenced by the ES interaction rather than the vdW interaction, both ES and vdW energies indicate that the preferred angle is  $R30^\circ$ .

The EM-h-BN can be transferred to any other substrates by the wet-transfer method with an aluminum etchant (Al-etchant: 68%  $\text{H}_3\text{PO}_4$ , 3%  $\text{HNO}_3$  and 5%  $\text{CH}_3\text{COOH}$  in water) (Figure 4a). In brief, (i) poly(methyl methacrylate) (PMMA) is spin-coated on the sample, and it is immersed in (ii) Al-etchants (for 10 min). (iii) Then, the floating PMMA film is transferred onto the target substrate, and (iv) PMMA is removed by acetone. Figure 4b shows that even a wafer-scale EM-h-BN sheet can be transferred onto a  $\text{SiO}_2$ /Si substrate. To investigate the capability of the transfer process, an AFM image was obtained of the EM-h-BN sheet transferred onto  $\text{SiO}_2$  (Figure 4c), and UV absorption spectra (Figure 4d) were obtained from pristine EM-h-BN (black) and EM-h-BN transferred on a quartz substrate (red). The AFM image and the unchanged intensity (red) in UV absorption spectra after the transfer process demonstrate that the entire EM-h-BN sheet is successfully transferred onto the target substrates. The top-view HR-TEM image of EM-h-BN in Figure 4e also reveals that EM-h-BN in our work has a single rotational orientation.

To test the capability of EM-h-BN as a dielectric material, metal–insulator–metal device structures were fabricated with  $1 \times 1 \mu\text{m}^2$  overlap of electrodes. The breakdown electric field of transferred EM-h-BN was observed as 7.8–9.2 MV/cm (Figure S9), which is even comparable with that measured in mechanically exfoliated h-BN samples (~10 MV/cm).<sup>45</sup> We finally studied transport characteristics of graphene devices using EM-h-BN. First, we fabricated top-gate graphene field effect transistors (FETs) on as-grown EM-h-BN/sapphire and bare sapphire (Figure S10) and measured the onset of the

Shubnikov-de Haas (SdH) oscillation which is a qualitative measure for sample quality (Figure 5a,b). A magnetic field where the SdH oscillation commences ( $B_{\text{SdH}}$ ) is a minimum field for a charge carrier to complete a cyclotron orbit without scattering. The device with graphene on EM-h-BN/sapphire exhibited  $B_{\text{SdH}}$  of about 3 T (Figure 5a), whereas that on sapphire  $B_{\text{SdH}}$  of about 7 T (Figure 5b). The situation is similar for electron and hole dopings. To further demonstrate the wide-range capability of our EM-h-BN as an insulating substrate, the EM-h-BN was transferred on 300 nm thick  $\text{SiO}_2/\text{Si}$  for bottom-gate graphene FET array devices (Figure 5c). The transport performance of graphene on EM-h-BN/ $\text{SiO}_2$  is better than that on  $\text{SiO}_2$ . (Figure 5d). The values of electron and hole mobility in graphene on EM-h-BN/ $\text{SiO}_2$  were calculated to be 14175 and 8670  $\text{cm}^2/(\text{V s})$ , respectively. These values are comparable with graphene on mechanically exfoliated h-BN,<sup>12</sup> and  $\sim 2.5$  (electron) and  $\sim 1.7$  (hole) times higher than graphene on  $\text{SiO}_2$  (5241 for electron and 5577  $\text{cm}^2/(\text{V s})$  for hole). Multilayer h-BN on oxide substrate prevents the p-doping of graphene from the oxide substrate, which is confirmed in the Raman spectra of graphene in Figure S11, and therefore, electron mobility is more improved than hole mobility. The negligible trapped charges in graphene devices on both of EM-h-BN/sapphire and EM-h-BN/ $\text{SiO}_2$  induce the enhanced performance of graphene device. Indeed, these results reveal that our EM-h-BN can be a useful insulating substrate for 2D materials.

In summary, we demonstrated wafer-scale and high-quality multilayer h-BN growth on a sapphire substrate by LPCVD. Spectroscopic and microscopic investigations revealed that the EM-h-BN has a wrinkle-free surface and AA' stacking order with a single orientation. A well-oriented superstructure of h-BN on sapphire was revealed, and theoretical calculations suggested that maximized vdW and ES interaction between h-BN and sapphire at  $R30^\circ$  results in the preferred orientation. The electron transport in a graphene FET on h-BN/ $\text{SiO}_2$  was much improved compared to that on  $\text{SiO}_2$ , which indicates the excellent capability of EM-h-BN as an insulating substrate. Because the EM-h-BN can be transferred to any substrate, our results will accelerate studies on vertical 2D heterostructures and 2D materials-based electronic devices.

## ASSOCIATED CONTENT

### Supporting Information

The Supporting Information is available free of charge on the ACS Publications website at DOI: [10.1021/acs.nanolett.6b01051](https://doi.org/10.1021/acs.nanolett.6b01051).

Detailed description of experimental method and additional information for modeling and simulation. (PDF)

## AUTHOR INFORMATION

### Corresponding Authors

\*E-mail: [shin@unist.ac.kr](mailto:shin@unist.ac.kr).

\*E-mail: [hslim@ibs.re.kr](mailto:hslim@ibs.re.kr).

### Author Contributions

H.S.S. and H.L. proposed the experiments and supervised the project. A.-R.J. and S.H. designed and performed the experiments. C.H., S.I.Y., G.K., H.Y.J., T.J.S., K.Y., and E.C. analyzed and discussed the experimental results. S.O.P., K.W., S.K.K., and N.P. calculated binding energy between h-BN and  $\text{Al}_2\text{O}_3$  surface using DFT and MD simulation. A.M., F.W., and K.S.N.

performed fabrication and measurements of devices. H.S.S., H.L., and A.-R.J. wrote the manuscript, and all authors discussed the results and commented on the manuscript.

### Notes

The authors declare no competing financial interest.

## ACKNOWLEDGMENTS

This work was supported by an NRF Grant (NRF-2014R1A2A2A01007136), IBS-R019-D1, and a Grant (Code 2011-0031630) from the Center for Advanced Soft Electronics under the Global Frontier Research Program through the National Research Foundation funded by the Ministry of Science, ICT, and Future Planning, Korea. K.S.N. acknowledges financial support from the Royal Society, ERC, and EU FP7 Graphene Flagship Project 604391.

## REFERENCES

- (1) Novoselov, K. S.; Geim, A. K.; Morozov, S. V.; Jiang, D.; Zhang, Y.; Dubonos, S. V.; Grigorieva, I. V.; Firsov, A. A. *Science* **2004**, *306*, 666–669.
- (2) Meric, I.; Han, M. Y.; Young, A. F.; Ozyilmaz, B.; Kim, P.; Shepard, K. L. *Nat. Nanotechnol.* **2008**, *3*, 654–659.
- (3) Radisavljevic, B.; Radenovic, A.; Brivio, J.; Giacometti, V.; Kis, A. *Nat. Nanotechnol.* **2011**, *6*, 147–150.
- (4) Wang, Q. H.; Kalantar-Zadeh, K.; Kis, A.; Coleman, J. N.; Strano, M. S. *Nat. Nanotechnol.* **2012**, *7*, 699–712.
- (5) Georgiou, T.; Jalil, R.; Belle, B. D.; Britnell, L.; Gorbachev, R. V.; Morozov, S. V.; Kim, Y. J.; Gholinia, A.; Haigh, S. J.; Makarovsky, O.; et al. *Nat. Nanotechnol.* **2012**, *8*, 100–103.
- (6) Liu, W.; Kang, J.; Sarkar, D.; Khatami, Y.; Jena, D.; Banerjee, K. *Nano Lett.* **2013**, *13*, 1983–1990.
- (7) Pradhan, N. R.; Rhodes, D.; Feng, S.; Xin, Y.; Memaran, S.; Moon, B. H.; Terrones, H.; Terrones, M.; Balicas, L. *ACS Nano* **2014**, *8*, 5911–5920.
- (8) Zunger, A.; Katzir, A.; Halperin, A. *Phys. Rev. B* **1976**, *13*, 5560–5573.
- (9) Golberg, D.; Bando, Y.; Huang, Y.; Terao, T.; Mitome, M.; Tang, C.; Zhi, C. *ACS Nano* **2010**, *4*, 2979–2993.
- (10) Lee, C.; Li, Q.; Kalb, W.; Liu, X. Z.; Berger, H.; Carpick, R. W.; Hone, J. *Science* **2010**, *328*, 76–80.
- (11) Dean, C. R.; Young, A. F.; Meric, I.; Lee, C.; Wang, L.; Sorgenfrei, S.; Watanabe, K.; Taniguchi, T.; Kim, P.; Shepard, K. L.; et al. *Nat. Nanotechnol.* **2010**, *5*, 722–726.
- (12) Gannett, W.; Regan, W.; Watanabe, K.; Taniguchi, T.; Crommie, M. F.; Zettl, A. *Appl. Phys. Lett.* **2011**, *98*, 242105.
- (13) Mak, K. F.; He, K.; Shan, J.; Heinz, T. F. *Nat. Nanotechnol.* **2012**, *7*, 494–498.
- (14) Young, A. F.; Dean, C. R.; Meric, I.; Sorgenfrei, S.; Ren, H.; Watanabe, K.; Taniguchi, T.; Hone, J.; Shepard, K. L.; Kim, P. *Phys. Rev. B: Condens. Matter Mater. Phys.* **2012**, *85*, 235458.
- (15) Withers, F.; Bointon, T. H.; Hudson, D. C.; Craciun, M. F.; Russo, S. *Sci. Rep.* **2014**, *4*, 4967.
- (16) Iqbal, M. W.; Iqbal, M. Z.; Khan, M. F.; Shehzad, M. A.; Seo, Y.; Park, J. H.; Hwang, C.; Eom, J. *Sci. Rep.* **2015**, *5*, 10699.
- (17) Britnell, L.; Gorbachev, R. V.; Jalil, R.; Belle, B. D.; Schedin, F.; Mishchenko, A.; Georgiou, T.; Katsnelson, M. I.; Eaves, L.; Morozov, S. V.; et al. *Science* **2012**, *335*, 947–950.
- (18) Britnell, L.; Gorbachev, R. V.; Geim, A. K.; Ponomarenko, L. A.; Mishchenko, A.; Greenaway, M. T.; Fromhold, T. M.; Novoselov, K. S.; Eaves, L. *Nat. Commun.* **2013**, *4*, 1794.
- (19) Watanabe, K.; Taniguchi, T.; Kanda, H. *Nat. Mater.* **2004**, *3*, 404–409.
- (20) Tay, R. Y.; Griep, M. H.; Mallick, G.; Tsang, S. H.; Singh, R. S.; Tumlin, T.; Teo, E. H.; Karna, S. P. *Nano Lett.* **2014**, *14*, 839–846.
- (21) Song, L.; Ci, L.; Lu, H.; Sorokin, P. B.; Jin, C.; Ni, J.; Kvashnin, A. G.; Kvashnin, D. G.; Lou, J.; Yakobson, B. I.; et al. *Nano Lett.* **2010**, *10*, 3209–3215.

- (22) Lee, K. H.; Shin, H. J.; Lee, J.; Lee, I. Y.; Kim, G. H.; Choi, J. Y.; Kim, S. W. *Nano Lett.* **2012**, *12*, 714–718.
- (23) Kim, K. K.; Hsu, A.; Jia, X.; Kim, S. M.; Shi, Y.; Hofmann, M.; Nezich, D.; Rodriguez-Nieva, J. F.; Dresselhaus, M.; Palacios, T.; et al. *Nano Lett.* **2012**, *12*, 161–166.
- (24) Kidambi, P. R.; Blume, R.; Kling, J.; Wagner, J. B.; Baehtz, C.; Weatherup, R. S.; Schloegl, R.; Bayer, B. C.; Hofmann, S. *Chem. Mater.* **2014**, *26*, 6380–6392.
- (25) Park, S.; Lee, J.; Kim, H. S.; Park, J.-B.; Lee, K. H.; Han, S. A.; Hwang, S.; Kim, S.-W.; Shin, H.-J. *ACS Nano* **2015**, *9*, 633–638.
- (26) Shi, Y.; Hamsen, C.; Jia, X.; Kim, K. K.; Reina, A.; Hofmann, M.; Hsu, A. L.; Zhang, K.; Li, H.; Juang, Z. Y.; et al. *Nano Lett.* **2010**, *10*, 4134–4139.
- (27) Kim, G.; Jang, A. R.; Jeong, H. Y.; Lee, Z.; Kang, D. J.; Shin, H. S. *Nano Lett.* **2013**, *13*, 1834–1839.
- (28) Park, J.-H.; Park, J. C.; Yun, S. J.; Kim, H.; Luong, D. H.; Kim, S. M.; Choi, S. H.; Yang, W.; Kong, J.; Kim, K. K.; et al. *ACS Nano* **2014**, *8*, 8520–8528.
- (29) Gao, Y.; Ren, W.; Ma, T.; Liu, Z.; Zhang, Y.; Liu, W.-B.; Ma, L.-P.; Ma, X.; Cheng, H.-M. *ACS Nano* **2013**, *7*, 5199–5206.
- (30) Kim, S. M.; Hsu, A.; Park, M. H.; Chae, S. H.; Yun, S. J.; Lee, J. S.; Cho, D.-H.; Fang, W.; Lee, C.; Palacios, T.; et al. *Nat. Commun.* **2015**, *6*, 8662.
- (31) Caneva, S.; Weatherup, R. S.; Bayer, B. C.; Blume, R.; Cabrero-Vilatela, A.; Braeuninger-Weimer, P.; Martin, M.-B.; Wang, R.; Baehtz, C.; Schloegl, R.; et al. *Nano Lett.* **2016**, *16*, 1250–1261.
- (32) Behura, S.; Nguyen, P.; Che, S.; Debbarma, R.; Berry, V. *J. Am. Chem. Soc.* **2015**, *137*, 13060–13065.
- (33) Lee, J.-H.; Lee, E. K.; Joo, W.-J.; Jang, Y.; Kim, B.-S.; Lim, J. Y.; Choi, S.-H.; Ahn, S. J.; Ahn, J. R.; Park, M.-H.; et al. *Science* **2014**, *344*, 286–289.
- (34) Gao, Y.; Liu, Z.; Sun, D.-M.; Huang, L.; Ma, L.-P.; Yin, L.-C.; Ma, T.; Zhang, Z.; Ma, X.-L.; Peng, L.-M.; et al. *Nat. Commun.* **2015**, *6*, 8569.
- (35) Yim, W. M.; Paff, R. J. *J. Appl. Phys.* **1974**, *45*, 1456.
- (36) Singh, S. K.; Neek-Amal, M.; Costamagna, S.; Peeters, F. M. *Phys. Rev. B: Condens. Matter Mater. Phys.* **2013**, *87*, 184106.
- (37) Frueh, S.; Kellett, R.; Mallory, C.; Molter, T.; Willis, W. S.; King'ondu, C.; Suib, S. L. *Inorg. Chem.* **2011**, *50*, 783–792.
- (38) Ismach, A.; Chou, H.; Ferrer, D. A.; Wu, Y.; McDonnell, S.; Floresca, H. C.; Covacevich, A.; Pope, C.; Piner, R.; Kim, M. J.; et al. *ACS Nano* **2012**, *6*, 6378–6385.
- (39) Paffett, M. T.; Simonson, R. J.; Papin, P.; Paine, R. T. *Surf. Sci.* **1990**, *232*, 286–296.
- (40) Sutter, P.; Lahiri, J.; Albrecht, P.; Sutter, E. *ACS Nano* **2011**, *5*, 7303–7309.
- (41) Alem, N.; Erni, R.; Kisielowski, C.; Rossell, M. D.; Gannett, W.; Zettl, A. *Phys. Rev. B: Condens. Matter Mater. Phys.* **2009**, *80*, 155425.
- (42) Ooi, N.; Rajan, V.; Gottlieb, J.; Catherine, Y.; Adams, J. B. *Modell. Simul. Mater. Eng.* **2006**, *14*, 515–535.
- (43) Wang, X.-G.; Chaka, A.; Scheffler, M. *Phys. Rev. Lett.* **2000**, *84*, 3650–3653.
- (44) Ahn, J.; Rabalais, J. *Surf. Sci.* **1997**, *388*, 121–131.
- (45) Lee, G.-H.; Yu, Y.-J.; Lee, C.; Dean, C.; Shepard, K. L.; Kim, P.; Hone, J. *Appl. Phys. Lett.* **2011**, *99*, 243114.